

Si₃N₄ Ceramics Sintered with Y₂O₃/SiO₂ and R₂O₃(ss)/SiO₂: A Comparative Study of the Processing and Properties

Sebastião Ribeiro*, Kurt Strecker

Dept. of Materials Engineering - DEMAR, Faculdade de Engenharia Química de Lorena
FAENQUIL, Bairro Mondezir, C.P. 116, 12600-000 Lorena, SP - Brazil

Received: March 27, 2003; Revised: March 21, 2004

A comparative study was made of Si₃N₄ sintered with two types of additives, namely, Y₂O₃/SiO₂ and R₂O₃(ss)/SiO₂, R₂O₃(ss) being a rare earth metal oxide in solid solution. The processing conditions for both types of Si₃N₄ were 14 vol% of additives and a sintering temperature of 1800 °C for 30, 60 and 240 min. To compare the efficiency of the additives in the material's sintering process, the density, flexural strength, fracture toughness and hardness were measured and the phase composition and microstructure determined. The results indicated that R₂O₃(ss)/SiO₂ as a sintering aid improved the material's high temperature strength and slowed down grain growth when compared with the Y₂O₃/SiO₂ additive.

Keywords: Si₃N₄, Y₂O₃, R₂O₃(ss), liquid phase sintering, properties

1. Introduction and Objectives

Silicon nitride (Si₃N₄) is a ceramic material whose physical, mechanical, thermal and chemical properties render it useful in many technological applications. Its main applications are in exhaust valves for combustion engines, heat exchange, seals, pistons and combustion chambers, as well as cutting tools¹⁻¹³.

Due to the covalent bonding nature of Si₃N₄, it can be sintered to a high final density only if additives are used to form a liquid phase. A very common additive for sintering covalent ceramics is yttrium oxide (Y₂O₃), which reacts with the silicon oxide (SiO₂) layer existing on the surface of Si₃N₄ particles or, when intentionally added, forms a silicate melt and promotes rapid sintering to high densities^{3, 4, 6, 8-10}. Other metal oxides such as MgO, Al₂O₃, Yb₂O₃, La₂O₃, Sc₂O₃, ZrO₂ have been also used as sintering additives for Si₃N₄ densification^{3, 4, 6, 9, 13, 14}.

Densification of Si₃N₄ by the liquid phase sintering (LPS-Si₃N₄) process occurs through dissolution of the alpha phase (α-Si₃N₄) into liquid and subsequent precipitation of the beta phase (β-Si₃N₄). The kinetics of the sintering process, the final microstructure and properties of the sintered Si₃N₄ are partly determined by the composition of the liquid phase^{2, 3, 5, 6, 8, 10, 11}.

Rare earth element compounds are extensively used in

many technological areas, e.g., in the preparation of high performance covalent ceramics, automotive catalysts, special alloys and components for the electronic industry. Their production in pure form is very expensive due to the extraction and purification operations¹²⁻¹⁴.

A process was developed at DEMAR-FAENQUIL to produce a rare earth oxide, R₂O₃(ss), from the mineral Xenotime. Alkaline fusion of Xenotime, acid leaching, oxalic precipitation and calcination are the main steps of the process to produce R₂O₃(ss). This material is an oxide mixture in the form of a solid solution and can be used as a sintering additive in the liquid phase sintering of silicon nitride ceramics^{12, 13, 15}.

Figure 1a shows the X-ray diffraction patterns of the R₂O₃(ss) and, for the sake of comparison, of an Y₂O₃-Yb₂O₃-Er₂O₃-Dy₂O₃ mechanical mixture (Fig. 1b). From these patterns and an analysis based on Trieste's program, it can be concluded that the natural oxide mixture forms a solid solution. This is possible due to the similar electronic configurations, ionic radii and crystalline structures of the rare earth ions^{2, 15}.

The objective of this work is to study the liquid phase sintering of Si₃N₄ ceramics using Y₂O₃/SiO₂ and R₂O₃(ss)/SiO₂ mixtures as additives and to compare the re-

*e-mail: sebastiao@demar.fauenquil.br

sulting microstructures and mechanical properties, to verify the possibility of replacing Y_2O_3 by $R_2O_3(ss)$.

2. Experimental Procedure

The starting powders were: α - Si_3N_4 - type LC12-SX, Hermann C. Starck (HCS), specific surface area $19 \text{ m}^2/\text{g}$, percentage of β - Si_3N_4 lower than 8 wt. (%), mean particle size $0.6 \mu\text{m}$ and minimum nitrogen content 38.2 wt. (%); Y_2O_3 , FINE type, Grade C, (HCS), specific surface area $10\text{-}16 \text{ m}^2/\text{g}$, Y_2O_3 minimum content 99.95 wt. (%); $R_2O_3(ss)$ (Table 1 shows the chemical analysis and other properties); and SiO_2 , Merck, purity 99.95% and particle size around $20 \mu\text{m}$.

Two powder mixtures were prepared by attrition milling for 4 h at 1000 rpm, using isopropyl alcohol, Merck, purity 99.5% (the exact compositions are listed in Table 2). The additive mixtures, Y_2O_3/SiO_2 or $R_2O_3(ss)/SiO_2$, were added in the stoichiometry of the disilicates, $Y_2Si_2O_7$ or $R_2Si_2O_7(ss)$, and kept constant at a 14 vol (%) relative to the amount of α - Si_3N_4 . The difference in weight between R_2O_3 and Y_2O_3 given in Table 2 is because of their distinct densities ($R_2O_3 = 6,51 \text{ g/cm}^3$ and $Y_2O_3 = 5,01 \text{ g/cm}^3$).

The powders were mixed, dried and sieved, after which the samples were compacted by cold isostatic pressing under 300 MPa to form $5 \times 5 \times 50 \text{ mm}^3$ parallelepipedic bars. Subsequently, the samples were sintered at $1800 \text{ }^\circ\text{C}$ for 30, 60 and 240 min in a nitrogen (White Martins, purity 99.996%) atmosphere under 1.8 MPa pressure in a graphite resistance furnace. The powder bed technique was used to minimize weight loss. The composition of the powder bed was: Si_3N_4 60 wt. (%), boron nitride (BN) 30 wt. (%) and SiO_2 10 wt. (%). The density of the sintered samples was determined by the immersion method. The phase composition was determined by X-ray diffraction and the samples microstructurally analyzed by scanning electron microscopy. The flexural strength was measured by the four-point bending method, hardness was determined by the Vickers's indentation method and fracture toughness by the Indentation Strength in Bending (ISB) method^{13,16}. The size of the samples used for all the mechanical tests was $3 \times 4 \times 50 \text{ mm}^3$. The equations used to calculate hardness (H_V), flexural strength (σ_f), and fracture toughness (K_{IC}) were:

$$H_V = 18,544 \cdot \frac{P}{d^2} \quad (1)$$

$$\sigma_f = \frac{3}{2} \cdot \frac{F(L_1 - L_2)}{b \cdot h^2} \quad (2)$$

$$K_{IC} = 0,59 \cdot \left(\frac{E}{H_V} \right)^{\frac{1}{8}} \cdot \left(\sigma_f \cdot P^{\frac{1}{3}} \right)^{\frac{3}{4}} \quad (3)$$

where H_V is the Vickers's hardness (GPa), P is the indentation load (g), d is the mean diagonal length (mm), s_f is the flexural strength (MPa), L_1 is the outer span (mm), L_2 is the inner span (mm), b is the specimen width (mm), h is the specimen's height (mm), K_{IC} is the fracture toughness ($\text{MPa} \cdot \text{m}^{1/2}$), E is Young's modulus (a value of 350 GPa has been assumed) and p is the indentation load.

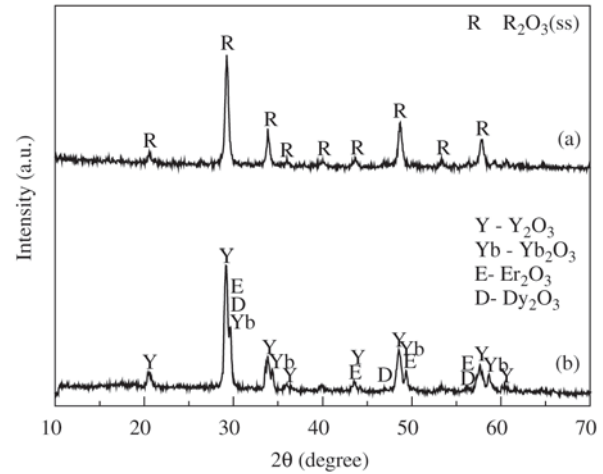


Figure 1. X-ray diffraction patterns of: a) solid solution rare earth oxide from natural Xenotime; b) mechanically mixed rare earth oxides.

Table 1. Composition of the $R_2O_3(ss)$ analyzed by Atomic Emission Spectrometry (ICP-AES), specific surface and mean particle size (X_{50}).

Oxide	wt. (%)	Oxide	wt. (%)
Y_2O_3	43.90	Sm_2O_3	0.41
Yb_2O_3	17.00	Pr_2O_3	0.27
Er_2O_3	13.60	CeO_2	0.18
Dy_2O_3	11.00	Nd_2O_3	0.18
Ho_2O_3	3.10	Eu_2O_3	0.06
Tm_2O_3	2.50	La_2O_3	0.04
Tb_2O_3	2.41	ZrO_2	1.06
Lu_2O_3	2.00	SiO_2	0.09
Gd_2O_3	1.73	Insoluble	0.56
Specific surface (m^2/g)		8.0	
Mean particle size X_{50} (μm)		1.74	

Table 2. Compositions of the prepared powder mixtures

Code	Composition (wt.%)			
	Si_3N_4	SiO_2	Y_2O_3	$R_2O_3(ss)$
SNY14	84.99	5.21	9.79	0.0
SNTR14	82.54	5.04	0.0	12.42

4. Results and discussion

Figure 2 shows the particle size distributions of the two powder mixtures. The mean particle sizes of the two powders, SNY14 and SNTR14, were about 0.8 μm and 1.3 μm , respectively. The average particle size of SNTR14 was larger than that of SNY14 because of the coarser R₂O₃(ss) additive in comparison to Y₂O₃. Both powder mixtures exhibited monomodal and wide particle size distributions. It can be concluded, from the results shown in Fig. 2, that the powder mixtures possessed good characteristics for pressing due to the wide range of particle size distribution. This distribution type follows Furnas's particle packing model, in which small particles are arranged in the spaces between the larger particles, contributing to reduce the porosity and pore size in the green body¹⁷.

Table 3 shows the relative densities of the green and sintered samples. The density of both mixtures increased as the sintering time increased. After sintering, the relative densities obtained with the R₂O₃(ss)/SiO₂ additive system were almost identical to those obtained with the Y₂O₃/SiO₂ additive system, indicating that R₂O₃ and Y₂O₃ produce a liquid that displays the same behavioral characteristics during the liquid phase sintering of Si₃N₄. The most important properties in this case are the liquid's wettability and viscosity.

Figure 3 (a-f) shows the microstructures of sintered Si₃N₄,

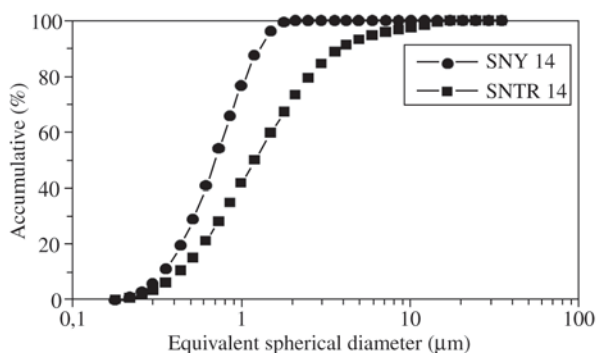


Figure 2. Particle size distributions of the SNY14 and SNTR14 powder mixtures.

revealing hexagonal β -Si₃N₄ grains in dark contrast, embedded in a secondary phase in light contrast, formed by the additives during sintering. The elongated grain morphology is a consequence of the phase transformation of $\alpha \rightarrow \beta$ -Si₃N₄ during the solution-precipitation process in the liquid phase sintering^{1-3,8,11-13}. As the sintering time increases, grain growth occurs by coalescence processes due to the different chemical potentials among smaller and larger Si₃N₄ grains.

The microstructural distribution and average grain size are illustrated in Fig. 4. Figure 4 (a-f) shows the grain size distribution obtained by photomicrographic analysis, as presented in Figure 3 (a-f), using the Quantikov program. The corners of the grains' sections were marked by hand on a transparency, and approximately 600 grains were measured for each sample (SNY14 and SNTR14).

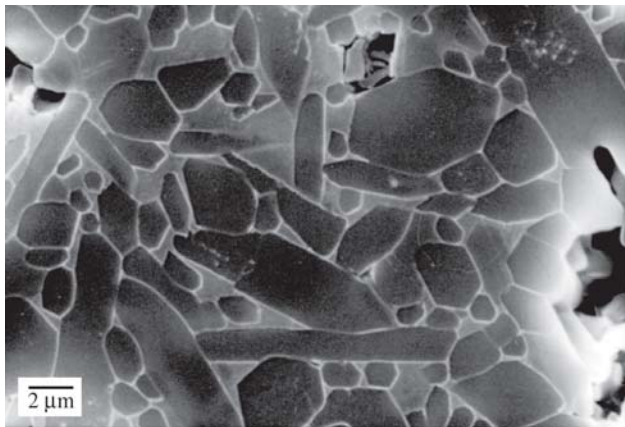
Based on the results shown in Fig. 3 and 4, it can be concluded that the grain size of both samples (SNY14 and SNTR14) gradually increased with increasing sintering time and that the samples sintered with Y₂O₃/SiO₂ produced slightly larger grains than the samples sintered with R₂O₃(ss)/SiO₂. The fact that the grain growth of β -Si₃N₄ was smaller in the R₂O₃(ss)/SiO₂ liquid than in the Y₂O₃/SiO₂ liquid can be attributed to the solution-precipitation process, in which the α -Si₃N₄ would be more soluble in liquid Y₂O₃/SiO₂, which would lead to greater grain growth through the precipitation of β -Si₃N₄⁵⁻¹³.

Table 4 summarizes the results of the flexural strength at room temperature, at 1200 °C, the strength retained at 1200 °C, the hardness, fracture toughness and crystalline phases. The retained strength is the correlation between the flexural strength at room temperature and 1200 °C.

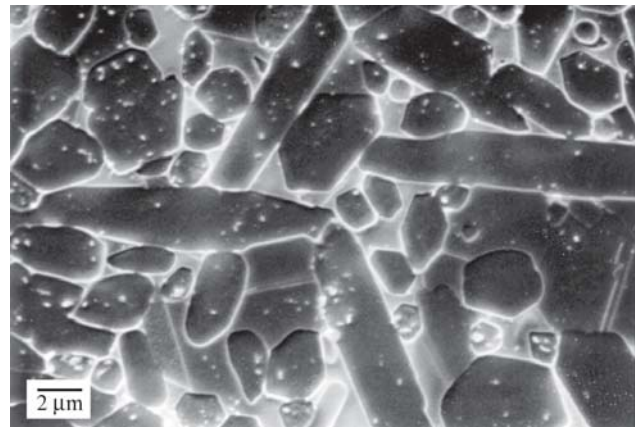
The values of room temperature and high temperature strengths of SNTR14 were slightly higher than those of the SNY14 mixture with identical sintering times and these values increased with increasing sintering time. The resistance retained at 1200 °C in every case was higher in samples containing R₂O₃(ss)/SiO₂ as additives than when compared to samples with Y₂O₃/SiO₂ additives. These properties can be explained by the debonding that should occur at the interface between the grains and the grain boundary phase. Interfacial debonding energy has been reported to be directly influenced by chemical bonding between the

Table 3. Theoretical density (mixture rule), and green and final relative densities after sintering at 1800 °C for 30, 60 and 240 min, of the SNY14 and SNTR14 samples.

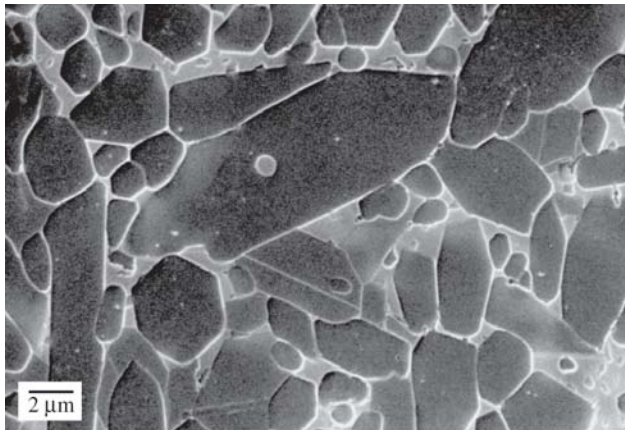
Code	Theoretical density(g/cm ³)	Relative density (T D.%)			
		Green compact	Sintering time (min)		
			30	60	240
SNY14	3,22	61,80 ± 0,28	89.39 ± 0,28	91.82 ± 0,31	95.45 ± 0,31
SNTR14	3,32	62,35 ± 0,31	90.21 ± 0,32	92.58 ± 0,33	96.14 ± 0,29



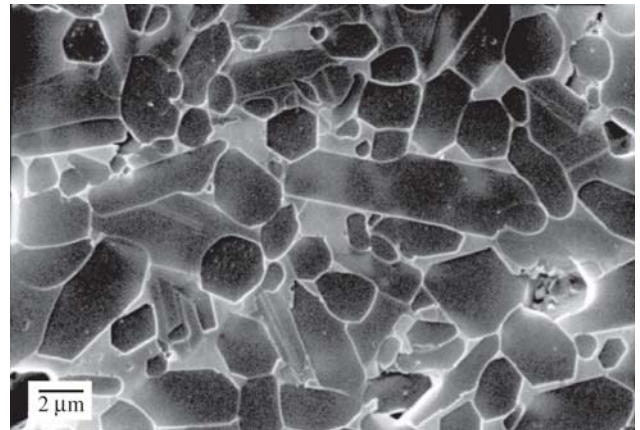
(a)



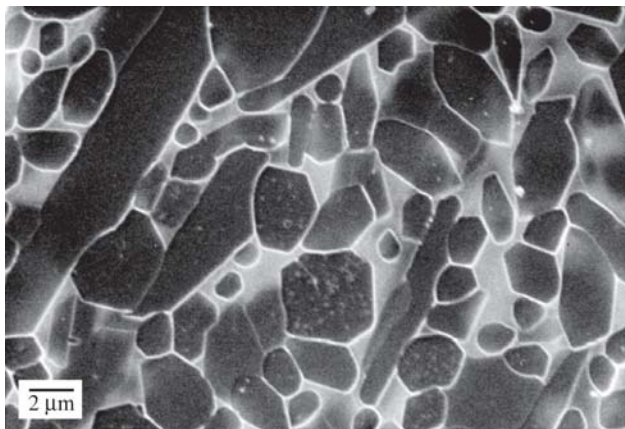
(b)



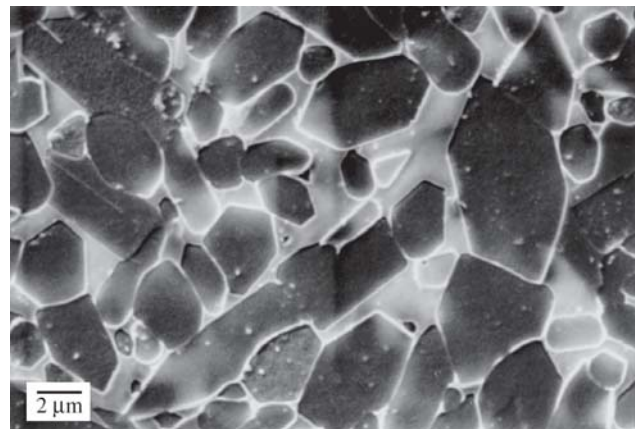
(c)



(d)



(e)



(f)

Figure 3. SEM micrographs of sintered SNY14 (a, b and c) and SNTR14 (d, e and f) samples. The samples were sintered at 1800 °C for 30 (a and d), 60 (b and e) and 240 (c and f) min, respectively.

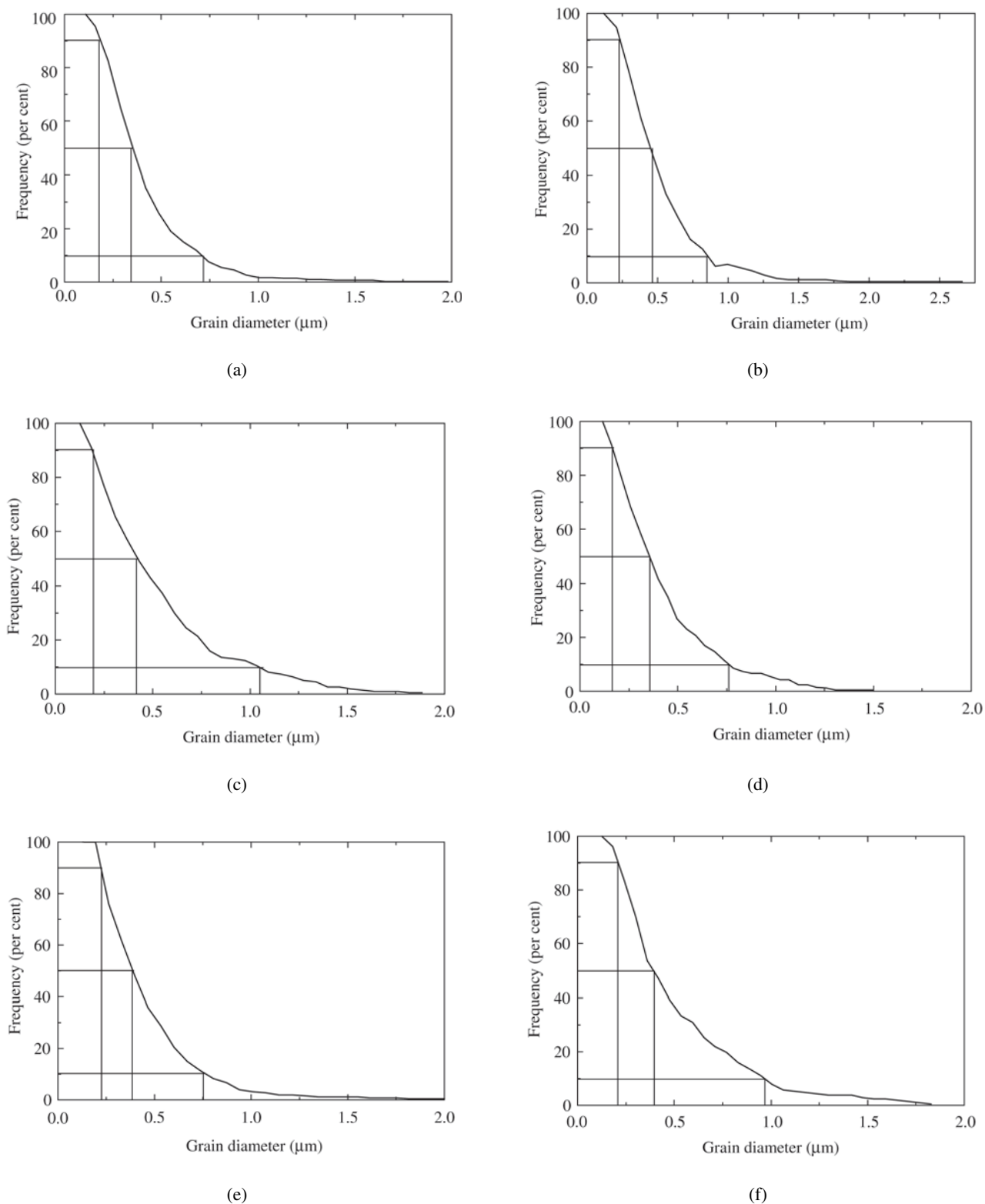


Figure 4. Grain size distributions revealed by the correlation between grain diameter and frequency for sintered SNY14 (a, b and c) and SNTR14 (d, e and f) samples. The samples were sintered at 1800 °C for 30 (a and d), 60 (b and e) and 240 (c and f) min, respectively.

Table 4. Properties of the SNY14 and SNTR14 samples sintered at 1800 °C for 30, 60 and 240 min.

Code	Parameters	Sintering time (min)		
		30	60	240
SNY14	σ_{25} (MPa)	402 ± 21	437 ± 21	469 ± 32
	σ_{1200} (MPa)	241 ± 10	231 ± 8	219 ± 20
	σ_{retained} (%)	60	53	47
	HV (GPa)	8.2 ± 0.3	9.6 ± 0.1	12.5 ± 0.6
	K_{IC} (MPa)	7.3 ± 0.7	7.1 ± 0.5	5.7 ± 0.1
	Phases	$\beta\text{-Si}_3\text{N}_4$; $\beta\text{-Y}_2\text{Si}_2\text{O}_7$	$\alpha\text{-Y}_2\text{Si}_2\text{O}_7$; $\text{Si}_2\text{N}_2\text{O}$	$\beta\text{-Si}_3\text{N}_4$; $\beta\text{-Y}_2\text{Si}_2\text{O}_7$
		$\alpha\text{-Y}_2\text{Si}_2\text{O}_7$; $\text{Si}_2\text{N}_2\text{O}$	$\beta\text{-Si}_3\text{N}_4$; $\beta\text{-Y}_2\text{Si}_2\text{O}_7$	$\text{Si}_2\text{N}_2\text{O}$
SNTR14	σ_{25} (MPa)	394 ± 26	491 ± 34	500 ± 47
	σ_{1200} (MPa)	289 ± 20	315 ± 16	303 ± 20
	σ_{retained} (%)	73	64	61
	HV (GPa)	8.6 ± 0.4	9.5 ± 0.2	12.2 ± 0.6
	K_{IC} (MPa)	7.5 ± 0.6	6.5 ± 0.3	5.8 ± 0.6
	Phases	$\beta\text{-Si}_3\text{N}_4$; $\beta\text{-R}_2\text{Si}_2\text{O}_7(\text{ss})$	$\beta\text{-Si}_3\text{N}_4$; $\beta\text{-R}_2\text{Si}_2\text{O}_7(\text{ss})$	$\beta\text{-Si}_3\text{N}_4$; $\beta\text{-R}_2\text{Si}_2\text{O}_7(\text{ss})$
		$\alpha\text{-R}_2\text{Si}_2\text{O}_7(\text{ss})$; $\text{Si}_2\text{N}_2\text{O}$	$\alpha\text{-R}_2\text{Si}_2\text{O}_7(\text{ss})$; $\text{Si}_2\text{N}_2\text{O}$	$\text{Si}_2\text{N}_2\text{O}$

grain boundary phase and the grains, and by the residual stress imposed on the interface as a result of mismatched thermal expansion³. The joining energy in the case of the $\text{R}_2\text{O}_3(\text{ss})/\text{SiO}_2$ -enriched system is higher than in the $\text{Y}_2\text{O}_3/\text{SiO}_2$ system.

Much of the literature states that the high temperature properties of liquid phase sintered Si_3N_4 is controlled by the viscosity of the amorphous intergranular phase. In yttrium silicates, the simultaneous presence of amorphous and crystalline phases has been observed in the intergranular phase and, since both materials were sintered with 14 vol% additive, which is a very large amount, the longer sintering time increased the amount of crystalline phase in the secondary phase, resulting in an almost constant strength for the SNTR14 at 1200 °C. In addition, the two materials displayed reduced strength at high temperatures, and the SEM micrographs confirm a typical Si_3N_4 microstructure with crystalline grains surrounded by amorphous/crystalline phase. The viscosity effect apparently controlled the mechanical behavior.

The hardness increased with increasing sintering time in every case. The two mixtures showed similar hardness values, although lower than those reported in the literature, mainly with short sintering times. The low hardness values were attributed to the samples' relatively low densities^{3, 10, 12} (Table 3).

The samples' fracture toughness for the same sintering times was similar, albeit showing decreasing values as the sintering time increased, a phenomenon that is explained

by the microstructure's grain morphology. As the sintering time increased, the grain morphology became more equiaxial, with a smaller aspect ratio, leading to less pronounced effects of crack-deflection and crack-bridging mechanisms. On the other hand, the samples with lower hardness values displayed greater fracture toughness, which is in agreement with the theory.

An X-ray analysis showed the presence of the $\beta\text{-Si}_3\text{N}_4$ and $\text{Si}_2\text{N}_2\text{O}$ phases in all the samples and at all the sintering times employed. Depending on the composition and sintering time, other phases such as $\alpha\text{-Y}_2\text{Si}_2\text{O}_7$, $\beta\text{-Y}_2\text{Si}_2\text{O}_7$, $\alpha\text{-R}_2\text{Si}_2\text{O}_7(\text{ss})$, $\beta\text{-R}_2\text{Si}_2\text{O}_7(\text{ss})$ were also present. The $\alpha\text{-Y}_2\text{Si}_2\text{O}_7$ phase transformed into the $\beta\text{-Y}_2\text{Si}_2\text{O}_7$ phase with longer sintering times. HRTEM analyses of the liquid phase sintered Si_3N_4 have shown that it is impossible to obtain a totally crystallized secondary phase³. The mechanical data, on the other hand, shows a strong possibility to found crystallized silicate and amorphous silicate mixtures.

5. Conclusions

The processing of the Si_3N_4 ceramics sintered with $\text{R}_2\text{O}_3(\text{ss})/\text{SiO}_2$ additives was identical to that with $\text{Y}_2\text{O}_3/\text{SiO}_2$ additive.

The flexural strength at room temperature and at 1200 °C, the fracture toughness and the hardness were identical or better with $\text{R}_2\text{O}_3(\text{ss})/\text{SiO}_2$ additive than with $\text{Y}_2\text{O}_3/\text{SiO}_2$ additive.

Si_3N_4 can be sintered successfully with $\text{R}_2\text{O}_3(\text{ss})/\text{SiO}_2$ additive.

Acknowledgements

The authors would like to thank the Instituto de Pesquisas Energéticas e Nucleares (IPEN), the Centro Técnico Aeroespacial (CTA) and the Max Planck Institute (MPI) for their support with image analyses, sample compaction and SEM analyses, respectively.

References

1. Lange, F.F.; Singhal, S.C.; Kuzwinski, R.C. *J. Am. Cer. Soc.*, v. 60, n.12, p. 249-252, 1977.
2. Cinibulk, M.K.; Thomas, G. *J. Am. Cer. Soc.*, v. 75, n. 8, p. 2044-2049, 1992.
3. Horng-Hwa Lu; Jow-Lay Huang, *Ceramics International*, v. 27, n. 6, p. 621-628, 2001.
4. Wen-Tse Lo; Jow-Lay Huang; Zan-Hon Shih; Ding-Fwu Lii; Chun-Te Li, *Materials Chemistry and Physics*, v. 73, n. 2-3, p. 123-128, 2002.
5. Chien-Cheng Liu, *Ceramics International*, v. 29, n. 7, p. 841-846, 2003.
6. Gao, L.; Yang, H.; Yuan, R.; Huang, P.; Xu, R.; Jung, J.Y.; Park, K.M., *Journal of Materials Processing Technology*, v. 115, n. 3, p. 298-301, 2001.
7. Wiederhorn, S.M.; Hockey, B.J.; French, J.D. *J.E. Cer. Soc.*, v. 19, n. 13-14, p. 2273-2284, 1999.
8. Guo, S.; Hirosaki, N.; Yamamoto, Y.; Nishimura, T.; Mitomo, M. *Scripta Materialia*, v. 45, n. 7, p. 867-874, 2001.
9. Guo, S.; Hirosaki, N.; Yamamoto, Y.; Nishimura, T.; Mitomo, M. *J. E. Cer. Soc.*, v. 23, n. 3, p. 537-545, 2003.
10. De Pablos; Osendi, M.I.; Miranzo, P. *Ceramics International*, v. 29, n. 7, p. 757-764 A, 2003.
11. Gopal, M.; Jonghe, L.C.; Thomas, G. *Acta Mater.*, v. 46, n. 7, p. 2401-2405, 1998.
12. Strecker, K.; Reinaldo, G.; Ribeiro, S.; Hoffmann, M.J.; *Materials Letters*, v. 45, n. 1, p. 39-42, 2000.
13. Ribeiro, S. Thesis, Faculdade de Engenharia Química de Lorena-Departamento de Engenharia de Materiais, p. 194, 1997.
14. Ribeiro, S.; Strecker, K.; Vernilli, F.J. *Cerâmica*, v.46, n. 297, p. 34-39, 2000.
15. Vernilli, F.J.; Vernill, D.C.; Ferreira, B.; Silva, G.; In press: *In anais 47 CBC*, 2003.
16. Hoffmann, M.J. *Herstellung von SiC-Whiskerverstärktem Si₃N₄ durch ein Kombiniertes Sinter-HIP-Verfahren. Stuttgart: Institut für Metallkunde der Univerfät Stuttgart, Max-Planck-Institut für Metallforschung*, p. 185, 1989.
17. Reed, J.D. *Introduction to the Principles of Ceramic Processing*, 2nd ed., p. 185-199, 1988.